Magnetic Resonance Imaging 63 (2019) 123–130

Contents lists available at ScienceDirect

Magnetic Resonance Imaging

journal homepage: www.elsevier.com/locate/mri

Original contribution

Carotid artery segmentation using level set method with double adaptive threshold (DATLS) on TOF-MRA images

Lian Luo[a,1], Shuai Liu[b,1], Xinyu Tong[a], Peirong Jiang[c], Chun Yuan[b,d], Xihai Zhao[b], Fei Shang[a,*]

[a] Department of Biomedical Engineering, School of Life Science, Beijing Institute of Technology, Beijing, China
[b] Department of Biomedical Engineering, Center for Biomedical Imaging Research, Tsinghua University School of Medicine, Beijing, China
[c] Department of Radiology, Fujian Medical University Union Hospital, Fujian, China
[d] Department of Radiology, University of Washington, Seattle, WA, USA

ARTICLE INFO

Keywords:
Carotid artery
Segmentation
Level set method
Double adaptive threshold
TOF-MRA

ABSTRACT

Purpose: This study aimed to propose a method to semi-automatically segment lumen of carotid artery on TOF-MRA images with well performance on images with weak boundary.

Methods: The proposed method modified traditional level set method with double adaptive threshold (DATLS). Two thresholds were calculated from probability density function of initial region of interest. Threshold Th1 was used to generate initial contour and threshold Th2 was used to control evolution by modifying energy function of the level set. The performance of the proposed method was tested on TOF-MRA images from CARE II study via using manual delineation as reference. Sixty cases were randomly selected to compare the performance of traditional level set with DATLS, all 283 cases were used to test the robustness of DATLS and 20 cases were used to compare the intra- and inter-operator reproducibility of manual delineation with DATLS. The Dice Similarity Coefficient, Mean Contour Distance and Hausdorff Distance between the proposed method and the manual segmentation were reported.

Results: Traditional level set failed to segment carotid artery on 13 cases because of over convergence. Compared to traditional level set, DATLS showed a higher DSC (0.88 ± 0.07 vs. 0.75 ± 0.15), lower MCD (0.48 ± 0.37 mm vs. 1.89 ± 2.24 mm) and HD (1.41 ± 1.11 mm vs. 4.59 ± 4.59 mm) in the remaining 47 cases. The average DSC, MCD and HD of DATLS on 283 cases were 0.87 ± 0.09, 0.64 ± 0.87 mm and 1.76 ± 2.23 mm, respectively. Compared to manual delineation, DATLS had better reproducibility on DSC (intra-operator: 0.97 ± 0.09 and inter-operator: 0.97 ± 0.09 vs. intra-operator: 0.91 ± 0.04 and inter-operator: 0.91 ± 0.04), as well as MCD (intra-operator: 0.08 ± 0.18 mm and inter-operator: 0.13 ± 0.52 mm vs. intra-operator: 0.35 ± 0.20 mm and inter-operator: 0.37 ± 0.19 mm) and HD (intra-operator: 0.30 ± 0.66 mm and inter-operator: 0.48 ± 1.38 mm vs. intra-operator: 0.99 ± 0.79 mm and inter-operator: 0.90 ± 0.85 mm).

Conclusion: Compared to traditional level set, DATLS out-performed on computing time, robustness and accuracy of segmentation on TOF-MRA. The proposed method using modified level set with double adaptive threshold might be a promising tool for lumen segmentation of carotid artery on TOF-MRA.

1. Introduction

Carotid artery atherosclerosis is a kind of systemic inflammatory disease that eventually causes arterial luminal stenosis and is closely correlated with cerebrovascular ischemic events, such as stroke or transient ischemia attack [1]. It has been well demonstrated that geometric characteristics of carotid arteries are associated with atherosclerotic disease [2,3]. Therefore, geometric evaluation of carotid arteries plays an important role in predicting the processing of atherosclerotic disease. Magnetic resonance angiography (MRA), such

Abbreviations: DATLS, level set method with double adaptive threshold; MRI, Magnetic Resonance Imaging; MRA, magnetic resonance angiography; TOF, time-of-flight; MIP, maximum intensity projection; LS, traditional level set method; DSC, Dice Similarity Coefficient; MCD, Mean Contour Distance; HD, Hausdorff Distance; CCA, common carotid artery; ICA, internal carotid artery; ECA, external carotid artery; CTA, Computed Tomography Angiography; PDF, probability density function

* Corresponding author at: Department of Biomedical Engineering, School of Life Science, Beijing Institute of Technology, Haidian District, Beijing 100081, China.
E-mail address: bit552sf@bit.edu.cn (F. Shang).

[1] These authors contributed equally to this work and should be considered as co-first authors.

https://doi.org/10.1016/j.mri.2019.08.002
Received 26 March 2019; Received in revised form 19 July 2019; Accepted 15 August 2019

as time-of-flight MR angiography (TOF-MRA), has been proved as an efficient imaging technique in assessing vascular morphology due to its high spatial resolution and large coverage [4,5]. TOF-MRA exploits inflow-enhancement effect. When flowing into stationary tissue, the fully magnetized (unsaturated) fresh blood exhibits significantly stronger signal than saturated tissue [6]. However, the signal of partially saturated blood becomes weak and the lumen of carotid artery exhibits weak boundary if blood flow is slow or disturbed. This phenomenon often occurs near vascular plaques and segmentation of vessel boundary is thus a challenge [7].

Segmentation of vessel lumen on MRA images is a critical step to characterize vascular morphology. However, traditional segmentation was to manually delineate the contour of vessel on each slice by radiologists and hence became time-consuming and heavily dependent on operator's experience. Therefore, some automatic and semi-automatic methods had been developed for fast segmentation. Among all segmentation methods, the level set method had been widely used on vessel segmentation because of its adaptability to clinical application [8]. Manniesing et al. [9] modified the level set method by combining the intensity and homogeneity features in carotid artery segmentation on Computed Tomography Angiography (CTA) images. Lu et al. [10] used a level set method with non-local robust statistics (NLRSS) to suppress noise in hepatic vessel segmentation. Hutter et al. [11] optimized the level set method to improve segmentation accuracy via incorporating skeleton information. Thus, the performance of level set methods in segmentation majorly relied on the selection of prior information and the construction of level set formulation.

Intensity information is a common prior information in segmentation. Many methods using intensity information had been proposed, such as K-means algorithm [12], region growing [13] and intensity statistics models [14–16]. Jodas et al. [12] combined K-means algorithm and active contour in coronary artery segmentation. Xiao et al. [13] applied region growing with detected seed points to segment cerebrovascular on multiple-feature fused enhanced images. Wang et al. [14] extracted the cerebral vessels with the threshold, which was calculated by comparing Gumbel distribution and unilateral normal distributions. Freiman et al. [15] constructed a prior intensity probability density function (PDF) for graph cut method to identify carotid vasculature in CTA. Considering significant contrast between the fully magnetized (unsaturated) fresh blood and saturated tissue, threshold might be an important information in carotid artery segmentation.

In the present study, an algorithm using level set with double adaptive threshold (DATLS) was proposed for semi-automatic segmentation of carotid artery on TOF-MRA images. The paper was further structured as follows: Section 2 described the traditional level set method and details of proposed algorithm; Section 3 showed the results of segmentation and the evaluation of DATLS performance. Discussion and conclusion were presented in Section 4 and Section 5 respectively.

2. Materials and methods

2.1. Dataset

A total of 283 carotid arteries from a study of Chinese Atherosclerosis Risk Evaluation (CARE II) [17] were used in the present study. The study protocol was approved by the Institution Review Board. The data were acquired in 13 medical centers and hospitals in China equipped with 3.0 Tesla MR scanner. Three-dimensional time-of-flight (3D-TOF) was scanned in the transverse direction and a standard protocol of 3D-TOF used the following parameters: in-plane field of view = 140 mm × 140 mm, acquisition matrix = 512 × 512, slice thickness = 2 mm, flip angle = 20°, number of slices = 48, TR = 20 ms, TE = 4.9 ms. The boundaries of lumen manually delineated by experienced radiologists were used as the golden standard for validation.

2.2. Traditional level set method

In traditional level set method proposed by Chunming Li et al. [18], a contour C is represented by zero-level curve of the function Φ, which is expressed as $C = \{(x, y) | \Phi(x, y) = 0\}$. The calculation process that the original contours deform into the blood vessel contour is given by the minimization of certain energy function with respect to Φ. The energy function is written as Eq. (1)

$$E(\phi) = \mu P(\phi) + \lambda L(\phi) + \nu A(\phi) \tag{1}$$

where $P(\phi)$ is internal energy to penalize the deviation of Φ using a signed distance function during curve deformation. The second term $L(\Phi)$ is a length-weighted term that smoothed the contour. The third term $A(\Phi)$ is an area-weighted term to maintain area. If $\nu > 0$, the contour shrinks, whereas if $\nu < 0$, it expands. it will stop at object boundaries. These energy functions are defined as below:

$$P(\phi) = \int_{\Omega} \frac{1}{2}(|\nabla\phi| - 1)^2 dxdy \tag{2}$$

$$L(\phi) = \int_{\Omega} g\delta(\phi)|\nabla\phi| dxdy \tag{3}$$

$$A(\phi) = \int_{\Omega} gH(-\phi) dxdy \tag{4}$$

where Ω is the 2D image domain, δ is the Dirac function, and H is the Heaviside function. g is an edge-detector which could be defined as Eq. (5),

$$g(x,y) = \frac{1}{1 + |\nabla I_G(x,y)|^2} \tag{5}$$

where $I_G(x,y) = I(x,y) * G_\sigma(x,y)$ represents the convolution of image I (raw image) and a Gaussian kernel with standard deviation σ. $g(x,y)$ ranges from 0 to 1. This point might be located near contour when $g(x,y)$ is close to 0 and homogenous background when $g(x,y)$ is close to 1.

2.3. DATLS

The segmentation of carotid artery images began at proximal common carotid artery and ended at distal branches. In first step, each slice was smoothed with Gaussian filter ($\sigma = 5$) and a circular ROI was generated with an initial point. Second, double adaptive threshold *Th1* and *Th2* were computed from PDF of intensity in ROI. *Th1* was used to get initial contour of segmentation and *Th2* was used to modify energy function in level set method. Third, contour of carotid artery was segmented with modified level set. An overview of DATLS was presented in Fig. 1 and details on three segmentation stages in each slice were described below.

2.3.1. Generation of initial ROI

Generation of initial ROI was different in the first slice, slices before and after bifurcation:

a) In the first slice at common carotid artery (CCA), an initial point was manually selected to generate a circular ROI with a radius of 25 pixels.
b) In slices from CCA to bifurcation, initial point was mass center of contour segmented in the previous slice and a circular ROI was generated with a diameter equal to 1.5 times major axis of segmented contour in the previous slice.
c) In slices from bifurcation to distal branches, initial point on external carotid artery (ECA) or internal carotid artery (ICA) was mass center of corresponding contour in the previous slice and a circular ROI with a diameter equal to 2 times major axis of corresponding contour in the previous slice.

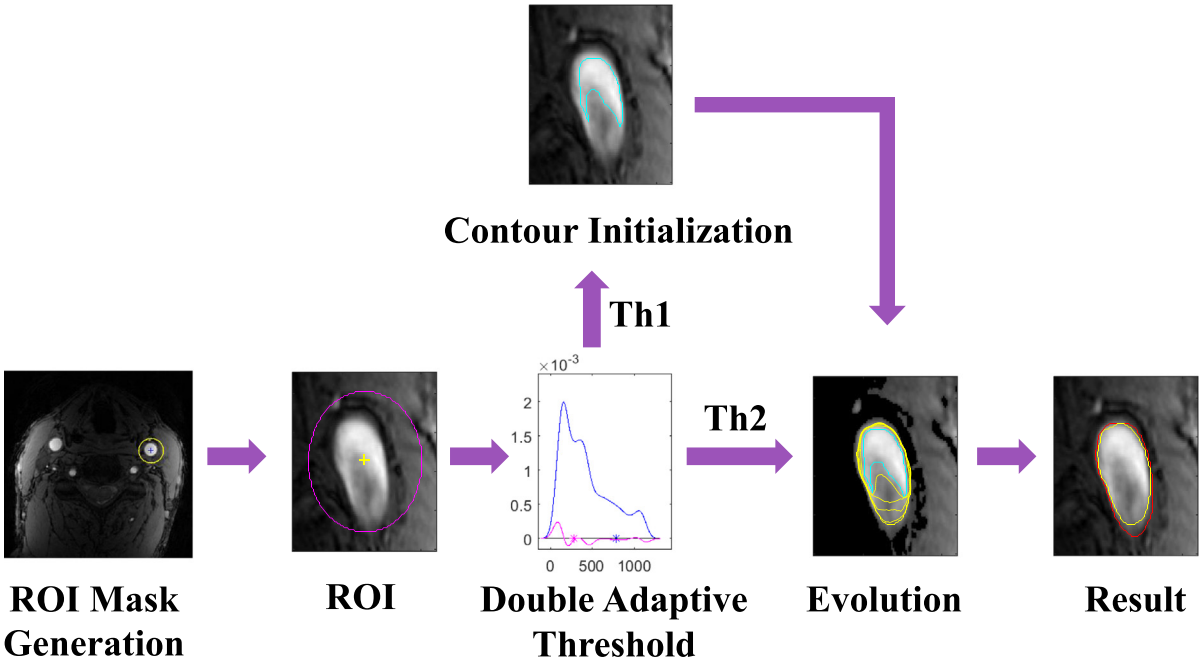

Fig. 1. Segmentation process in each slice. In the figure of probability density function (PDF), blue asterisk indicates the threshold Th1, Purple asterisk indicates the threshold Th2. (For interpretation of the references to colour in this figure legend, the reader is referred to the web version of this article.)

2.3.2. Double adaptive threshold calculation

After initial ROI was generated, double adaptive threshold was calculated from PDF of intensity in ROI. *Th1* was the minimum between two largest peaks in PDF and *Th2* was the first value greater than -1e-4 after lowest value in derivative of PDF.

For images with clear vessel boundaries, the PDF of ROI was characterized as a bimodal shape in which the first peak represented background region and the second one represented the vessel region. Segmentation with *Th1* could well distinguish vessel from background area. On images with weak boundary, *Th1* became very high and thus segmented region was smaller than vessel region. Therefore, on images with weak boundary, *Th1* was corrected by the thresholds of the previous two slices in order to move initial contour close to boundary. Correction equation for *Th1* was as follows,

$$Th1_i = \begin{cases} Th1_i & (|Th1_i - Th1_{i-1}| \le 100) \\ \dfrac{Th1_{i-2} + Th1_{i-1} + Th1_i}{3} & (100 < |Th1_i - Th1_{i-1}| \le 200) \\ \dfrac{3 * Th1_{i-1} + Th1_i}{4} & (|Th1_i - Th1_{i-1}| > 200) \end{cases} \quad (6)$$

where *i* represented the current slice. After *Th1* correction, *Th1* was not the valley point between two largest peaks (Fig. 1 and Fig. 4).

On images with weak boundary, lower or higher *Th2* may occur due to the irregular shape of PDF, which would contribute to over-expansion of segmented contour or under-segmentation. Therefore, *Th2* of the previous slice was used to correct current *Th2* and correction equation was as follows:

$$Th2_i = \begin{cases} Th2_i & (|Th2_i - Th2_{i-1}| \le 100) \\ \dfrac{Th2_{i-1} + Th2_i}{2} & (|Th2_i - Th2_{i-1}| > 100) \end{cases} \quad (7)$$

Moreover, difference between *Th1* and *Th2* should be larger than 100, a further correction for *Th1* was execute according to equation as below,

$$Th1_i = \max(Th1_i, Th2_i + 100) \quad (8)$$

In slices with branches, two *Th1s* were calculated from PDF of the ECA and ICA while *Th2* was the minimum of *Th2s* of ECA and ICA.

2.3.3. Modified level set

In this step, initial contour was generated by *Th1* at first. Segmented areas with pixels < 20 were excluded. In slices with branches, two initial contours generated on the ECA and ICA branches, respectively. Then, contour expanded using level set with modified area-weighted term by *Th2*. The area-weighted term modified by *Th2* in energy function was defined as:

$$A(\phi) = \int_\Omega sgn(I - Th2) * gH(-\phi)dxdy \quad (9)$$

where *sgn* represented Symbolic function and *sgn(I−Th2)* functioned as a mask preventing contour from over-expansion. Final energy function was written as below:

$$E(\phi) = \mu \int_\Omega \frac{1}{2}(|\nabla\phi| - 1)^2 dxdy + \lambda \int_\Omega g\delta(\phi)|\nabla\phi|dxdy + \nu' \int_\Omega sgn(I - Th2) * gH(-\phi)dxdy \quad (10)$$

If the current segmentation results did not have overlapped area with the results of the previous slice, the contour would be abandoned.

2.4. Evaluation

To evaluate the performance of DATLS, the vessel was divided into four segments with same length equal to 10 mm (Fig. 2): (1) proximal CCA (pCA1); (2) vessel from proximal CCA to bifurcation (pCA2); (3) vessel from bifurcation to distal branches (dCA1); (4) distal branches (dCA2).

Dice Similarity Coefficient (DSC), Mean Contour Distance (MCD) and Hausdorff Distance (HD) were used to evaluate the performance of two methods and calculated in each segment according to the equations below [19,20],

$$Dice\ Similarity\ Coefficient\ (DSC) = \frac{2 * (A \cap B)}{A + B} \quad (11)$$

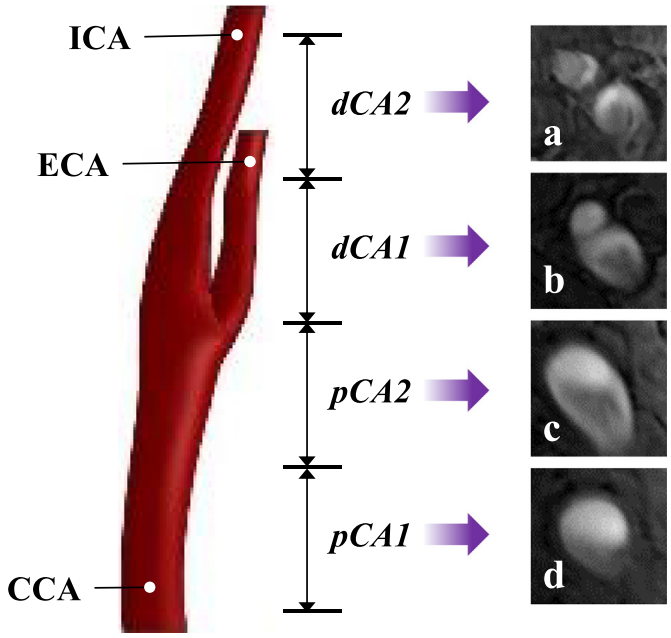

Fig. 2. Segments of carotid artery. CCA: common carotid artery; ICA: internal carotid artery; ECA: external carotid artery; dCA2: segments at the distal carotid bifurcation; dCA1: segments just after carotid bifurcation; pCA2: segments just before carotid bifurcation; pCA1: segments at the proximal common carotid artery; a, b, c, d represent TOF images from different cases with weak boundaries in four segments, respectively.

Mean Contour Distance (*MCD*)

$$= \frac{1}{2}\left(\frac{1}{|\partial A|}\sum_{a\in\partial A} d(a,\partial B) + \frac{1}{|\partial B|}\sum_{b\in\partial B} d(b,\partial A)\right) \quad (12)$$

Hausdorff Distance (*HD*)

$$= \max\left(\max_{a\in\partial A}(\min(d(a,\partial B))), \max_{b\in\partial B}(\min(d(b,\partial A)))\right) \quad (13)$$

where d represented absolute distance, A and B represented segmentation results of two method.

Additionally, 20 cases were randomly selected for intra- and inter-operator reproducibility analysis. Two experienced operators (> 10 years) analyzed each carotid artery by manual delineation and DATLS. Intra-operator reproducibility was analyzed via comparing two contours delineated by same radiologist with 2 month's interval. Inter-operator reproducibility was analyzed via comparing the delineations from two radiologists, who were blinded to each other.

3. Experiments and results

Segmentation was implemented in MATLAB R2016a environment on the computer with a 3.4GHz Core (TM) i7–2600 CPU and 8GB memory. The proposed method was compared with traditional level set method proposed by Li et al. [18]. In traditional level set method, μ was fixed at 0.23, while λ and ν should be adjusted manually for each case. For the proposed method, μ = 0.23, λ = 4000, ν = −700. The iteration number in two methods were both 60.

In present study, all cases were used to evaluate robust performance of DATLS and 60 cases were randomly selected to compare the performance of traditional level set method with DATLS. Segmentation with traditional level set cost 15–20 min for each case, while calculation cost of DATLS was < 4 min.

Among 60 cases, 13 cases failed in contour segmentation with traditional level set on account of excessive convergence. The comparisons between two methods using remaining 47 cases were shown in Fig. 4 and Table 1. Compared to traditional level set, DATLS showed a higher DSC (0.88 ± 0.07 vs. 0.75 ± 0.15), lower MCD (0.48 ± 0.37 mm vs. 1.89 ± 2.24 mm) and HD (1.41 ± 1.11 mm vs. 4.59 ± 4.59 mm).

Table. 2 showed the performance of DATLS for 283 carotid arteries. The mean of DSC, MCD and HD were 0.87 ± 0.09, 0.64 ± 0.87 mm and 1.76 ± 2.23 mm, respectively. Among four segments, dCA2 exhibited lowest DSC (0.80 ± 0.12) and highest MCD (1.05 ± 1.49 mm) and HD (2.73 ± 3.78 mm), while pCA2 showed highest DSC (0.90 ± 0.05) and pCA1 showed lowest MCD (0.45 ± 0.29 mm) and HD (1.05 ± 0.67 mm).

The intra- and inter-operator reproducibility of manually delineation and DATLS were summarized in Table 3. Compared to manually delineation, DATLS showed a higher DSC (intra-operator: 0.97 ± 0.09 and inter-operator: 0.97 ± 0.09 vs. intra-operator: 0.91 ± 0.04 and inter-operator: 0.91 ± 0.04), lower MCD (intra-operator: 0.08 ± 0.18 mm and inter-operator: 0.13 ± 0.52 mm vs. intra-operator: 0.35 ± 0.20 mm and inter-operator: 0.37 ± 0.19 mm) and HD (intra-operator: 0.30 ± 0.66 mm and inter-operator: 0.48 ± 1.38 mm vs. intra-operator: 0.99 ± 0.79 mm and inter-operator: 0.90 ± 0.85 mm).

Table 2
Evaluation of the segmentation on 283 carotid arteries.

	Mean ± SD (n = 283)		
	DSC	MCD (mm)	HD (mm)
pCA1	0.89 ± 0.06	0.45 ± 0.29	1.05 ± 0.67
pCA2	0.90 ± 0.05	0.48 ± 0.24	1.44 ± 0.66
dCA1	0.87 ± 0.08	0.58 ± 0.64	1.82 ± 1.81
dCA2	0.80 ± 0.12	1.05 ± 1.49	2.73 ± 3.78
average	0.87 ± 0.09	0.64 ± 0.87	1.76 ± 2.23

DSC: dice similarity coefficient; MCD: mean contour distance; HD: Hausdorff distance.

4. Discussion

In this study, a modified level set with double adaptive threshold (DATLS) was proposed to semi-automatically delineate the contour of carotid artery on TOF-MRA images. Comparing to traditional level set,

Table 1
Comparison of traditional level set method and DATLS.

	LS vs DATLS (n = 47) (Mean ± SD)		
	DSC	MCD (mm)	HD (mm)
pCA1	0.84 ± 0.09 vs 0.90 ± 0.05	0.57 ± 0.49 vs 0.41 ± 0.25	1.53 ± 1.17 vs 1.02 ± 0.60
pCA2	0.80 ± 0.10 vs 0.90 ± 0.05	1.02 ± 0.80 vs 0.47 ± 0.23	2.89 ± 1.58 vs 1.45 ± 0.72
dCA1	0.67 ± 0.15 vs 0.88 ± 0.05	2.95 ± 2.19 vs 0.42 ± 0.23	7.13 ± 4.46 vs 1.43 ± 0.90
dCA2	0.62 ± 0.18 vs 0.82 ± 0.09	3.90 ± 3.15 vs 0.61 ± 0.61	8.77 ± 6.02 vs 1.74 ± 1.74
average	0.75 ± 0.15 vs 0.88 ± 0.07	1.89 ± 2.24 vs 0.48 ± 0.37	4.59 ± 4.59 vs 1.41 ± 1.11

DSC: dice similarity coefficient; MCD: mean contour distance; HD: Hausdorff distance.

Table 3
Reproducibility.

	Mean ± SD (n = 20)			
	Manual		Semi-automated	
	Intra-observer	Inter-observer	Intra-observer	Inter-observer
DSC	0.91 ± 0.04	0.91 ± 0.04	0.97 ± 0.09	0.97 ± 0.09
MCD (mm)	0.35 ± 0.20	0.37 ± 0.19	0.08 ± 0.18	0.13 ± 0.52
HD (mm)	0.99 ± 0.79	0.90 ± 0.85	0.30 ± 0.66	0.48 ± 1.38

DSC: dice similarity coefficient; MCD: mean contour distance; HD: Hausdorff distance.

DATLS exhibited robust performance via using the intensity features as a constraint during evolution.

In normal carotid artery, PDF of ROI is characterized as a bimodal shape. The largest peak in PDF represents background (background peak) while the second largest peak represents enhanced blood flow in vessel (flow peak). Thus, the minimum between two peaks would be a threshold functioning well on distinguishing background from vessel. However, turbulence and disturbed flow are common in bifurcation or carotid artery with plaque and contributable to inhomogeneity of signal in vessel as well as weak boundary of carotid artery on TOF images. Therefore, PDF of ROI is not bimodal in carotid artery with weak boundary because a peak (false peak) might appear between background peak and flow peak or flow peak is not obvious. When false peak appears, *Th1* is low and initial contour will be larger than vessel boundary and when flow peak is not obvious, *Th1* is high and initial contour will be far smaller than vessel boundary. In most carotid arteries with weak boundary, flow peak cannot be obviously detected. In the present study, evolution of contour is to expand from inner to boundary and adaptive threshold *Th2* controls deformation of contour. A lower *Th2* will lead to an over-expanded initial contour and hence failure on segmentation, while a higher *Th2* will slow expansion of contour and not reach to true boundary when iteration is over. Therefore, a threshold correction using information of the previous slice was proposed to eliminate the influence caused by turbulence and disturbed flow in the present study. Abnormal *Th1* could be prevented by considering similarity of features between two adjacent slices.

Additionally, signal inhomogeneity in vessel makes it a challenge to detect boundary of vessel during evolution. Considering mechanism of TOF-MRA, vessel wall which is also stationary tissue exhibits similar feature with background and this similarity leads to difference of PDF between stationary tissue and blood flow on images. In the present study, the first zero point after minimum in derivation of PDF was set as a threshold to control the evolution of contour. However, PDF of ROI will fluctuate between background peak and flow peak in carotid artery with weak boundary. This fluctuation favors the profile of inhomogeneity of signal in vessel and leads to appearance of abnormal peak in PDF of stationary tissue. Therefore, *Th2* was also corrected by *Th2* in the previous slice in this study. Besides, evolution will be constrained if *Th1* is close to *Th2*. As a solution, a further correction of difference between *Th1* and *Th2* was executed to guarantee segmentation with level set.

Fig. 3 exhibited adaptive adjustment of *Th1* and *Th2* along from proximal CCA to distal branches. In the present study, threshold segmentation with *Th1* reduced evolution time via generating an initial contour close to true boundary. Energy term modified by *Th2* controlled

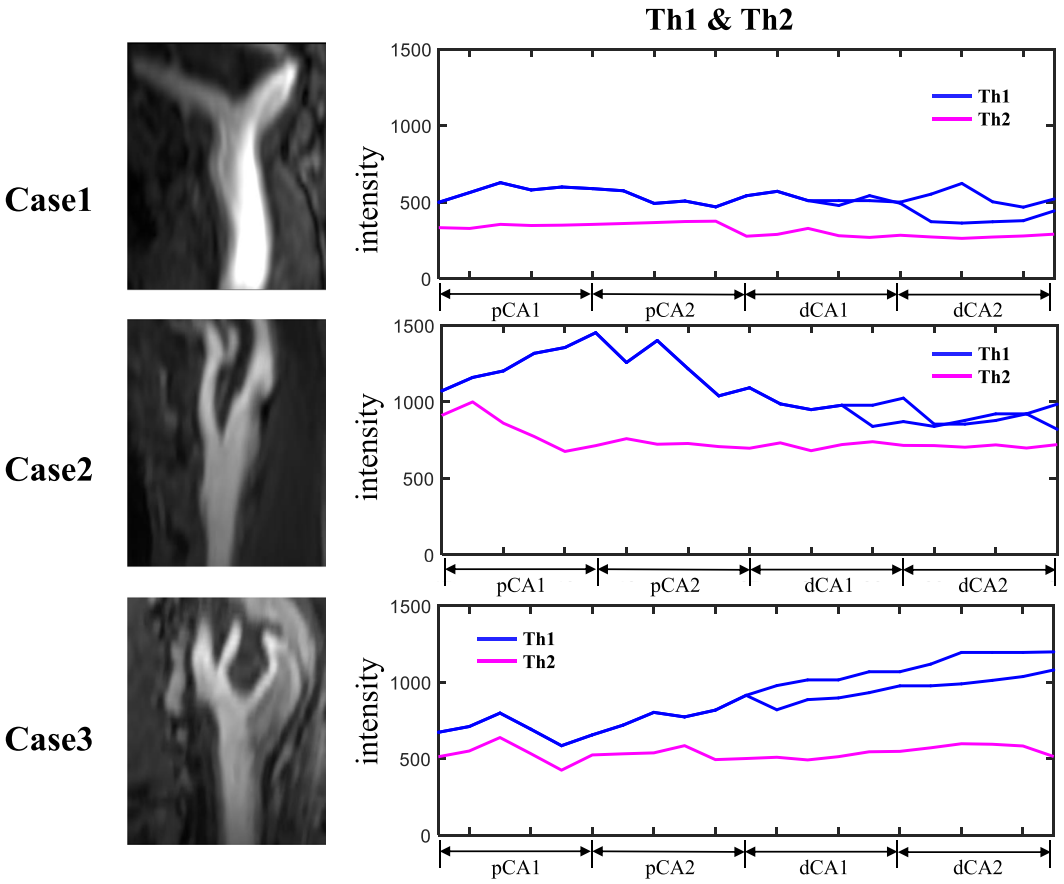

Fig. 3. Examples of vessels with its threshold Th1 and Th2 from the proximal common carotid artery to the distal branch vessels. The blue lines represent the values of Th1 and the purple lines represent the values of Th2. (For interpretation of the references to colour in this figure legend, the reader is referred to the web version of this article.)

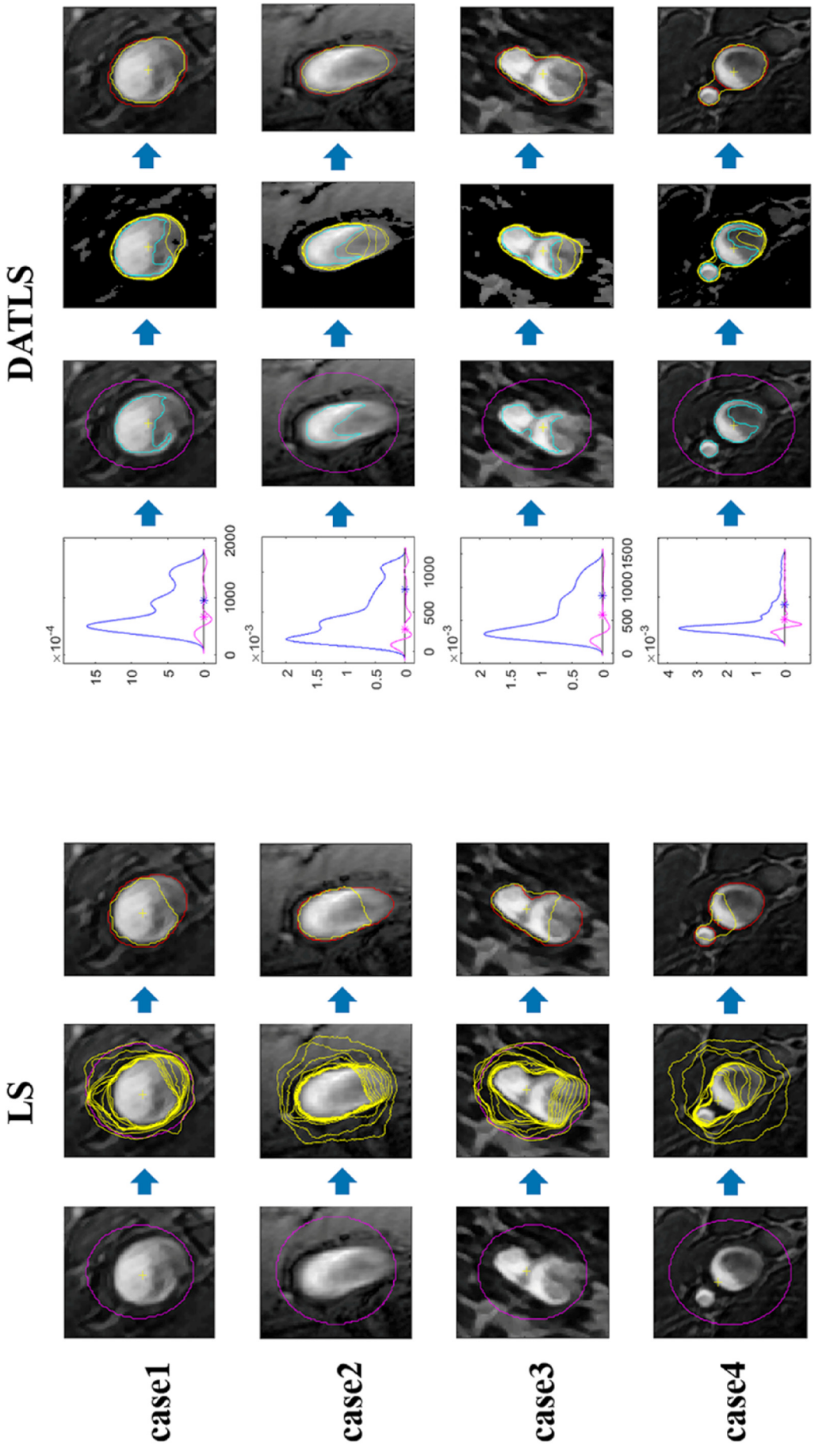

Fig. 4. The comparison of segmentation performance between two level set methods at four segments on the carotid arteries with weak boundary. The purple contours are the ROI boundaries which are the initial contours for traditional level set method. The yellow contours represent the active contours and final segmented results. The red contours represent the gold standard. (For interpretation of the references to colour in this figure legend, the reader is referred to the web version of this article.)

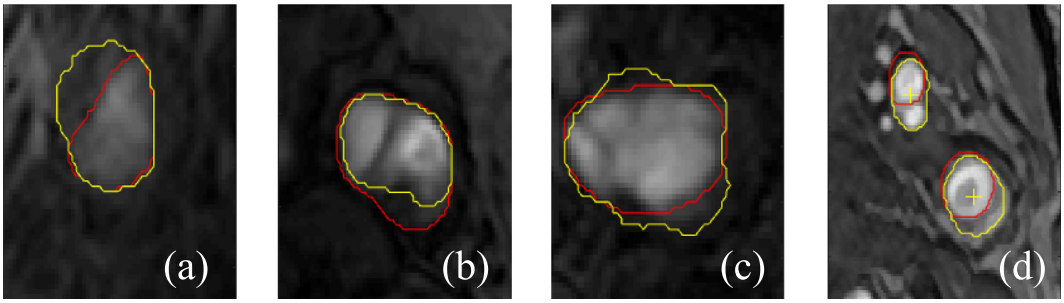

Fig. 5. Examples of results that were not accurately segmentated. The red contours represent gold standards delineated by experienced radiologists, the yellow contours represent the results calculated by DATLS. (For interpretation of the references to colour in this figure legend, the reader is referred to the web version of this article.)

active contour deformation and terminated evolution at true boundary. Deformation of contour in traditional level set largely depended on parameters setting, while DATLS was non sensitive to parametric variation. Besides, DATLS also out-performed on calculation cost and segmentation accuracy compared with traditional level set (Table. 1) and robustness (Table. 2). In addition, compared to manual delineation, DATLS showed better intra- and inter-operator reproducibility. As mentioned above, we believed that DATLS might be a potential method for carotid artery segmentation.

Table. 2 summarized performance of DATLS on DSC, MCD and HD at each vessel segment. It showed that the performance of DATLS at pCA1 and pCA2 was better than that at dCA1 and dCA2. According to inflow-enhancement effect, signal intensity of blood flow on TOF-MRA is associated with velocity of blood flow and angle between blood flow and imaging plane. At proximal CCA which is perpendicular to imaging plane, contrast between blood flow and stationary tissue is strong. However, signal intensity becomes weak in distal branches after bifurcation due to decreased velocity and inclined direction of blood flow [11,21,22]. Moreover, plaques often present near bifurcation and disturb blood flow nearby [3,23,24]. Therefore, at segments dCA1 and dCA2, weak boundary always appeared and segmentation result was not as well as that at pCA1 and pCA2.

This study suffered from several limitations. First, DATLS performed not well if image quality was poor or signal intensity of blood flow was inhomogeneous (Fig. 5). In fact, it's also a challenge for radiologists to delineate truth ground in some cases which lumen boundary was not obvious. Second, DATLS was a semi-automatic method in which a point was selected manually to generate ROI in first slice. In addition, segmentation result in the previous slice could provide prior information, however, bias might be accumulated and subsequent segmentation would be influenced. This accumulated bias was contributable to poor segmentation at segments dCA1 and dCA2 comparing with pCA1 and pCA2. Last, only TOF-MRA was used in the present study. The segmented contour might be closer to truth ground via using other imaging sequences, such as T1-weighted or T2-weighted.

5. Conclusion

In our study, the well performance of modified level set with double adaptive threshold has been validated by testing on CARE II study dataset. Our results suggested that the proposed method might be a promising method for semi-automatic segmentation of carotid artery on TOF-MRA.

Acknowledgements

None.

Funding sources

This study is funded by the grants of the National Natural Science Foundation of China [grant number: 81771825], Beijing Municipal Science and Technology Commission [grant number: D17110003017003], and Chinese Ministry of Science and Technology [grant number: 2017YFC1307904].

Declaration of interest statement.

None.

References

[1] Liu XS, Zhao HL, Cao Y, Lu Q, Xu JR. Comparison of carotid atherosclerotic plaque characteristics by high-resolution black-blood MR imaging between patients with first-time and recurrent acute ischemic stroke. AJNR Am J Neuroradiol 2012;33(7):1257–61. https://doi.org/10.3174/ajnr.A2965.

[2] Thomas JB, Antiga L, Che SL, Milner JS, Steinman DAH, Spence JD, et al. Variation in the carotid bifurcation geometry of young implications for geometric risk of atherosclerosis. Stroke 2005;36(11):2450–6. https://doi.org/10.1161/01.STR.0000185679.62634.0a.

[3] Lee SW, Antiga L, Spence JD, Steinman DA. Geometry of the carotid bifurcation predicts its exposure to disturbed flow. Stroke 2008;39(8):2341–7. https://doi.org/10.1161/STROKEAHA.107.510644.

[4] Gao S, Klooster Ronald van't, Kitslaar PH, Coolen Bram F, Berg Alexandra M van den, Smits Loek P, et al. Learning-based automated segmentation of the carotid artery vessel wall in dual-sequence MRI using subdivision surface fitting. Med Phys 2017;44(10). https://doi.org/10.1002/mp.12476.

[5] Yamada K, Song Y, Hippe DS, Sun J, Dong L, Xu D, et al. Quantitative evaluation of high intensity signal on MIP images of carotid atherosclerotic plaques from routine TOF-MRA reveals elevated volumes of intraplaque hemorrhage and lipid rich necrotic core. J Cardiovasc Magn Reson 2012;14(1):81. https://doi.org/10.1186/1532-429X-14-81.

[6] Adame IM, van der Geest RJ, Wasserman BA, Mohamed MA, Reiber JH, Lelieveldt BP. Automatic segmentation and plaque characterization in atherosclerotic carotid artery MR images. MAGMA 2004;16(5):227–34. https://doi.org/10.1007/s10334-003-0030-8.

[7] Sousa LC, Castro CF, António CC, Santos AMF, Dos Santos RM, Castro PMAC, et al. Toward hemodynamic diagnosis of carotid artery stenosis based on ultrasound image data and computational modeling. Med Biol Eng Comput 2014;52(11):971–83. https://doi.org/10.1007/s11517-014-1197-z.

[8] Li C, Xu C, Gui C, Fox MD. Level set evolution without re-initialization: A new variational formulation. Computer vision and pattern recognition. IEEE computer society conference on IEEE Xplore CVPR 2005, vol. 2005;1. 2005. p. 430–6. https://doi.org/10.1109/CVPR.2005.213.

[9] Manniesing R, Schaap M, Rozie S, Hameeteman R, Vukadinovic D, van der Lugt A, et al. Robust CTA lumen segmentation of the atherosclerotic carotid artery bifurcation in a large patient population. Med Image Anal 2010;14(6):759–69. https://doi.org/10.1016/j.media.2010.05.001.

[10] Lu S, Huang H, Liang P, Chen G, Xiao L. Hepatic vessel segmentation using variational level set combined with non-local robust statistics. Magn Reson Imaging 2017;36:180–6. https://doi.org/10.1016/j.mri.2016.10.021.

[11] Hutter J, Hofmann HG, Grimm R, Greise A, Saake M, Hornegger J, et al. Prior-based automatic segmentation of the carotid artery lumen in TOF MRA (PASCAL). Medical image computing and computer-assisted intervention – MICCAI 2012 Springer Berlin Heidelberg; 2012. https://doi.org/10.1007/978-3-642-33418-4_63.

[12] Jodas DS, Pereira AS, Tavares JMRS. Automatic segmentation of the lumen region in intravascular images of the coronary artery. Med Image Anal 2017;40:60–79. https://doi.org/10.1016/j.media.2017.06.006.

[13] Xiao R, Ding H, Zhai F, Zhou W, Wang G. Cerebrovascular segmentation of TOF-MRA based on seed point detection and multiple-feature fusion. Comput Med Imaging Graph 2018;69:1–8. https://doi.org/10.1016/j.compmedimag.2018.07.002.

[14] Wang R, Li C, Wang J, Wei X, Li Y, Zhu Y, et al. Threshold segmentation algorithm for automatic extraction of cerebral vessels from brain magnetic resonance angiography images. J Neurosci Methods 2015;241:30–6. https://doi.org/10.1016/j.jneumeth.2014.12.003.

[15] Freiman M, Joskowicz L, Broide N, Natanzon M, Nammer E, Shilon O, et al. Carotid vasculature modeling from patient CT angiography studies for interventional procedures simulation. Int J Comput Assist Radiol Surg 2012;7(5):799–812. https://doi.org/10.1007/s11548-012-0673-x.

[16] Jodas DS, Pereira AS, R S Tavares JM. Lumen segmentation in magnetic resonance images of the carotid artery. Comput Biol Med 2016;79:233–42. https://doi.org/10.1016/j.compbiomed.2016.10.021.

[17] Zhao X, Li R, Hippe DS, Hatsukami TS, Yuan C, CARE-II Investigators. Chinese atherosclerosis risk evaluation (CARE II) study: a novel cross-sectional, multicentre study of the prevalence of high-risk atherosclerotic carotid plaque in Chinese patients with ischaemic cerebrovascular events — design and rationale. Stroke Vasc Neurol 2017;2(1):15–20. https://doi.org/10.1136/svn-2016-000053.

[18] Li C, Xu C, Gui C, Fox MD. Level set evolution without re-initialization: A new Variational formulation. Computer vision and pattern recognition, 2005. CVPR 2005: IEEE computer society conference on IEEE Xplore vol. 1. 2005. p. 430–6. https://doi.org/10.1109/CVPR.2005.213.

[19] Dice L. Measures of the amount of ecologic association between species. J Ecol 1945;26:297. https://doi.org/10.2307/1932409.

[20] Bai W, Sinclair M, Tarroni G, Oktay O, Rajchl M, Vaillant G, et al. Automated cardiovascular magnetic resonance image analysis with fully convolutional networks. J Cardiovasc Magn Reson 2018;20(1):65. https://doi.org/10.1186/s12968-018-0471-x.

[21] Saloner D. The AAPM/RSNA physics tutorial for residents. An introduction to MR angiography. Radiographics 1995;15(2):453–65. https://doi.org/10.1148/radiographics.15.2.7761648.

[22] Wehrli FW. Time-of-flight effects in MR imaging of flow. Magn Reson Med 1990;14:187–93. https://doi.org/10.1002/mrm.1910140205.

[23] Sousa LC, Castro CF, António CC, Santos AF, dos Santos AM, Castro PM, et al. Haemodynamic conditions of patient-specific carotid bifurcation based on ultrasound imaging. Computer Methods in Biomechanics & Biomedical Engineering Imaging & Visualization 2014;2(3):157–66. https://doi.org/10.1080/21681163.2013.875486.

[24] Debrey SM, Yu H, Lynch JK, Lövblad KO, Wright VL, Janket SJ, et al. Diagnostic accuracy of magnetic resonance angiography for internal carotid artery disease: a systematic review and meta-analysis. Stroke 2008;39(8):2237–48. https://doi.org/10.1161/STROKEAHA.107.509877.